Hindawi
International Journal of Optics
Volume 2023, Article ID 9715482, 10 pages
https://doi.org/10.1155/2023/9715482

Research Article

The Multiple Scattering of Laser Beam Propagation in Advection Fog and Radiation Fog

Qiang Xu,[1] **Yunhua Cao**,[1] **Yuanyuan Zhang**,[1] **Shaohui Yan**,[2] **Yiping Han**,[1] **and Zhensen Wu**[1]

[1]*School of Physics and Optoelectronic Engineering, Xidian University, Xi'an 710071, China*
[2]*The State Key Laboratory of Transient Optics and Photonics, Xi'an Institute of Optics and Precision Mechanics, Chinese Academy of Sciences, Xi'an 710119, China*

Correspondence should be addressed to Zhensen Wu; wuzhs@mail.xidian.edu.cn

Received 31 March 2022; Revised 29 October 2022; Accepted 8 December 2022; Published 10 January 2023

Academic Editor: Paramasivam Senthilkumaran

The laser beams were scattered and attenuated when they propagate in fogs for laser communication, laser remote sensing detection. For different density and droplets distribution of fogs, the laser scatter and attenuation are different, the correspond mechanism need thorough investigation. The characteristics of laser beam scattering in different types of fogs are studied based on the droplet size characteristics of advection fog and radiation fog, the scattering coefficients of droplets with different laser wavelengths(0.86 μm, 0.91 μm, 1.06 μm, 1.3015, and 10.6 μm) are calculated, the multi scattering of laser beam is studied by the Monte Carlo method, the propagation path and scattering direction of photons is analyzed, relations between asymmetry factor, albedo of fog droplets, and the visibility are presented, and the forward scattering intensity and the backward scattering intensity versus scattering angle are gotten and discussed.

1. Introduction

Fogs contains small water droplets, these droplets suspend in the air, and they attenuate laser beam; fogs have adverse effects on optical communication, lidar, remote sensing, etc. Many scientists have conducted researches in this field. Nebuloni derived relations between an extinction coefficient and visibility of fog for near, mid, and far-IR (infrared) light transmission of free-space optic communications; the extinction coefficients in the visible 0.55 μm, the near IR 1.2 μm, and the mid IR 3.7 μm are comparable to and roughly twice as much as that in the far-IR10.6 μm when visibility is less than a few hundred meters [1]. Grabner and Kvicera measured the receiving power after beam scattering in free-space optical communication system at wavelengths of 0.83 μm and 1.55 μm; several fog attenuation events were observed on experimental paths. Important relations between fog microphysical parameters, atmospheric visibility, optical signal attenuation and bit error ratio based on measured data are presented in this case study [2]. Nebuloni and Capsoni used liquid water content and visibility to identify laser attenuation characteristics in fog; results show that visibility is almost proportional to fog attenuation at short wavelengths but not in the far-IR region [3]. Ijaz et al. proposed a new wavelength dependent empirical model to predict the spectrum attenuation of free-space optical communication systems operating at visible and near infrared wavelengths under fog and smoke in a laboratory condition, for the same fog and smoke conditions, it was found that the attenuation of light is almost linearly decreasing when laser wavelength increase from visible to NIR range [4]. Grabner and Kvicera analyzed the multiple scattering of light and the impulse response of optical channel in rain and fog for free-space optical links. Simulations show that optical attenuation of the multiple scattering due to rain is about two times lower than predicted by single scattering approach [5]. Mori and Marzano proposed an atmospheric water particles scattering model (a unified microphysically oriented atmospheric particle scattering model) and simulated the scattering effects on free-space optics links, scattering, absorption, and extinction coefficients and the asymmetry factor are numerically simulated for each particle

class, and then parametrized with respect to particle water content, fall rate, and visibility, spanning from visible to infrared wavelengths [6]. Wu et al. analyzed the changes of extinction coefficients and visibilities based on short and long time lidar data, and evaluated the free-space optical communication link for different wavelengths under the sea surface environment. The horizontal extinction coefficients and visibilities are obtained by inverting the collected data. On this basis, the free-space optical communication link availabilities of the 850 and 1550 nm links are evaluated during the observation period [7]. Al Naboulsi and Sizun presented results on fog attenuation at wavelengths 650, 850, and 950 nm; they have compared the experimental data with our fog attenuation models; the advection and the radiation one deduced from FASCODE (Fast Atmospheric Signature Codes). This comparison clearly shows that, for the three studied wavelengths, their models lead to the best fits for the measured data [8]. Shapiro used ultrashort (femtosecond duration) light pulses for line-of-sightfree-space optical (FSO) communication through fog; their study show that scattering-induced multipath spread is less than the reciprocal of the scattering-induced doppler spread [9]. Su et al. investigates scintillation and fog attenuation effects for THz and IR signals by measuring bit error rates (BER), signal power, and phase front distortions [10]. Shah et al. established an engineering model of laser transmission in fog, and compared with other models, selected nine models including theoretical and empirical models, which were simulated in MATLAB, and the comparison results were discussed [11]. Wang et al utilized a large quantity of high-quality water vapor lidar data collected by a multifunction Raman lidar system, investigated the air mass trajectories, variations of water vapor over Xi'an. The results indicate that local airflow trajectories mainly affect water vapor transport below the boundary layer, and that these flows are closely related to the formation of fog and haze events in the Xi'an area [12]. Di et al. proposed a method to measure the aerosol and fog particle size distribution by optimizing scattering angle and wavelengths; seven wavelengths for extinction coefficients and five wavelengths for forward scattering coefficients were chosen for the retrieval of particle size distribution in the measurement [13]. Zeng et al. studied the propagation of linear and circular polarization in fog, and comparing their transmission characteristic with different condition, investigated the transmission performance of circular and linear polarization in variable foggy environments, exploring the impact of the detection range in particular [14]. Zhang et al. calculated on the reflection and transmission of light propagating through sea fog by dividing fog into different layers with different refractive indices. The scattering processes of the radiation in the poly-disperse sea fog layer are traced in their improved Monte Carlo (MC) simulation. They provide more accurate calculations on the reflection and transmission when radiation propagates through poly-disperse sea fog media of two different refractive indices [15]. Vasseur and Gibbins developed an experimental method to infer the physical characteristics of fog from concurrent attenuation measurements at millimeter, infrared, and visible wavelengths; a gamma function comprised of three parameters is assumed for the drop size distribution. Simulations of fog attenuation based on the inferred drop size distribution are found in excellent agreement with the measurements [16]. Al Naboulsi et al. investigated laser system performance in the advection and convection fog in the 0.4 μm to 15 μm spectral zone, the author also proposes a fast transmission relations based on an exact Mie theory calculation valid in the 0.69 μm to 1.55 μm spectral bands [17].

The visibility is an important parameter of fog, which can be measured directly and quickly; however, the correlation between fog droplet parameter and the visibility and the scattering parameters of beams changing with fog's visibility for different beams' wavelengths have not been reported by now. The current laser transmission model is simple, for laser with different wavelength, it is urgent to study scattering character of fog particles and the multiple scattering of low visibility fog.

In this paper, we propose on the correlation between visibility and fog droplet parameter, such as distribution, droplet extinction coefficient, and asymmetry factor of different types of fogs. Based on this, using Monte Carl method, for infrared laser beams with different wavelength, the multi scattering of laser beam in fogs is studied. The coefficients versus visibility and scattering intensity distribution versus scattering angle are studied in detail.

2. The Particle Size Distribution of Fog

The fog particles are small water droplets. The particle size distribution function is given as follows [8, 14]:

$$n(r) = ar^2 e^{-br}, \tag{1}$$

where n is the number of droplets per unit volume and unit radius and r is the droplet radius. Other parameters are determined by the size distribution of fog.

Visibility of fog is related to the optical attenuation γ, which is expressed as follows [18]:

$$V = \frac{3.912}{\gamma}. \tag{2}$$

The optical attenuation γ is as follows [16]:

$$\gamma = 4.343 \cdot 10^{-3} \int_0^{\infty} Q_e(r)\pi r^2 n(r) dr^{dB/km}, \tag{3}$$

where Q_e (r) is the optical extinction efficiency. The dimensions of fog droplets are much greater the visible optical wavelength, so Q_e (r) of fog droplets can be consider as 2 [17]. γ can be written as follows [16]:

$$\begin{aligned}\gamma &= 4.343 \cdot 10^{-3} \int_0^{\infty} 2\pi r^2 \cdot ar^2 e^{-br} dr \\ &= \frac{8.686 \cdot 10^{-3} \pi a 4!}{b^5} \frac{\mathrm{d}B}{km}.\end{aligned} \tag{4}$$

Liquid water content is expressed as follows[5]:

$$W = \frac{4}{3}\pi\rho \int_0^{\infty} r^3 n(r) \mathrm{d}r, \tag{5}$$

where $\rho \sim 10^6$ g/m^3.

With equation (1), W is rewritten as follows:

$$W = 10^6 \frac{4\pi}{3} \int_0^\infty a r^5 e^{-br} \mathrm{d}r = \frac{4\pi 5! a}{3b^6} \times 10^6. \quad (6)$$

By equations (2)–(6), a and b is expressed by V and W as follows:

$$a = \frac{9.781}{V^6 W^5} 10^{15}, b = \frac{1.304}{VW} 10^4. \quad (7)$$

The droplet concentration can be obtained as follows:

$$N = \int_0^\infty n(r)\mathrm{d}r = \frac{2a}{b^3} = \frac{8.222}{V^3 W^2} \cdot 10^3. \quad (8)$$

The model radius corresponds to the peak value of droplet size distribution curve as follows:

$$r_o = \frac{2}{b} = 1.534 \cdot 10^{-4} VW. \quad (9)$$

The average radius of droplet size distribution is as follows:

$$\overline{r} = \frac{1}{N} \int_0^\infty r n(r)\mathrm{d}r = \frac{3}{b} = \frac{3}{2} r_0 = 2.301 \cdot 10^{-4} VW. \quad (10)$$

According to different regions, fog can be divided into two types, advection fog and radiation fog. For advection fog, relations between the liquid water content W and the V is shown as follows[19]:

$$W = (18.35V)^{-1.43} = 0.0156 V^{-1.43} \left(\frac{g}{m^3}\right). \quad (11)$$

For radiation fog, it is shown as follows:

$$W = (42.0V)^{-1.54} = 0.0316 V^{-1.54} \left(\frac{g}{m^3}\right). \quad (12)$$

For advection fog, droplet size distribution is calculated from equations (1), (7), (11), and (12), as follows:

$$\begin{aligned} n_{a\,dv}(r) &= 1.059 \cdot 10^7 V^{1.15} r^2 \exp\left(-0.8359 V^{0.43} r\right) \\ &= 3.73 \cdot 10^5 W^{-0.804} r^2 \exp\left(-0.2392 W^{-0.301} r\right). \end{aligned} \quad (13)$$

For radiation fog, droplet size distribution is as follows:

$$\begin{aligned} n_{rad}(r) &= 3.104 \cdot 10^{10} V^{1.7} r^2 \exp\left(-4.122 V^{0.54} r\right) \\ &= 5.400 \cdot 10^7 W^{-1.104} r^2 \exp\left(-0.5477 W^{-0.351} r\right). \end{aligned} \quad (14)$$

3. Scattering Coefficient of Fog Droplets

Using Mie scattering theory, the extinction coefficient Q_e, scattering coefficient Q_s, absorption coefficient Q_a, asymmetry factor g, and single albedo w_0 of a single particle can be calculated as follows [20]:

$$\begin{aligned} Q_e &= \frac{2}{\alpha_\lambda^2} \sum_{n=1}^\infty (2n+1)\{\mathrm{Re}(a_n + b_n)\}, \\ Q_s &= \frac{2}{\alpha_\lambda^2} \sum_{n=1}^\infty (2n+1)\left(|a_n|^2 + |b_n|^2\right), \\ Q_a &= Q_e - Q_s, \\ w_0 &= \frac{Q_s}{Q_e}, \\ g &= \frac{4}{\alpha_\lambda^2 Q_s} \sum_{n=1}^\infty \left\{ \frac{n(n+1)}{n+1} \mathrm{Re}\left(a_n a_{n+1}^* + b_n b_{n+1}^* + \frac{2n+1}{n(n+1)} \mathrm{Re}\left(a_n b_n^*\right) \right) \right\}. \end{aligned} \quad (15)$$

where α_λ is particle size parameter and a_n and b_n are Lorentz-Mie scattering coefficients.

With the above formula, we obtain coefficients of single fog droplet. However, in practical application, we need to consider the size distribution of fog droplets; the average coefficients are to be calculated [21].

The average extinction coefficient is as follows:

$$\langle \sigma_e \rangle = \frac{\pi \int_0^\infty r^2 Q_e(r) n(r) dr}{N}. \quad (16)$$

The average scattering coefficient is as follows:

$$\langle \sigma_s \rangle = \frac{\pi \int_0^\infty r^2 Q_s(r) n(r) dr}{N}. \quad (17)$$

The average absorbtion coefficient is as follows:

$$\langle \sigma_a \rangle = \frac{\pi \int_0^\infty r^2 Q_a(r) n(r) dr}{N}. \quad (18)$$

The droplet concentration is as follows:

$$N = \int_0^\infty n(r)\mathrm{d}r. \quad (19)$$

The average single albedo is as follows:

$$\langle w_0 \rangle = \frac{\langle \sigma_s \rangle}{\langle \sigma_e \rangle}. \tag{20}$$

The average asymmetry factor is as follows:

$$\langle g \rangle = \frac{\int_0^\infty r^2 Q_s(r) g(r) n(r) dr}{\int_0^\infty r^2 Q_s(r) n(r) dr}. \tag{21}$$

With the size distribution of the fog, we can calculate the average coefficients of fogs.

4. Monte Carlo Method for Laser Beam Propagation in Fog

The Monte Carlo method can be employed for the complex case of light scattering [15, 22, 23], the incident photon and the particles of the medium are regarded as the dispersive particles interacting with each other. There are scattering and absorption during the transmission of photons in the random medium. In the multiple scattering processes, it can be described by Markov process. The transmission history of photons is expressed as a phase space point $s = (\tau, \mu, \varphi)$, and the particle transport equation can be expressed as follows [22]:

$$I(s) = I_{ri}(s) + \int I(s') K(s' \longrightarrow s) \mathrm{d}s'. \tag{22}$$

Obviously,

$$\int I_{ri}(s) \mathrm{d}s = \int_0^\infty e^{-\tau} \mathrm{d}\tau \iint_{4\pi} \delta(\mu - 1) \delta(\phi) \mathrm{d}\mu \mathrm{d}\phi = 1. \tag{23}$$

Equation (22) has the Neumann series solution as follows:

$$I(s) = \sum_{m=0}^{\infty} I_m(s), \tag{24}$$

$$\begin{aligned} I_0(s) &= (s), \\ I_1(s) &= \int I_0(s_0) K(s_0 \longrightarrow s) \mathrm{d}s, \\ &\cdots\cdots\cdots\cdots\cdots\cdots \\ I_m(s) &= \int I_{m-1}(s_{m-1}) K(s_{m-1} \longrightarrow s) \mathrm{d}s_{m-1}, \\ &= \int \cdots \int I_0(s_0) K(s_0 \longrightarrow s_1) \\ &\quad \ldots K(s_{m-1} \longrightarrow s) \mathrm{d}s_{m-1} \ldots \mathrm{d}s_1 \mathrm{d}s_0. \end{aligned} \tag{25}$$

The integral operator shows that photons have experienced a transmission and collision. $I_0(s)$ means these photons propagating in the medium without collision, and $I_m(s)$ means the photons arriving at the phase space points after m collisions.

The probability model can well describe equation (25). Here, the event is that photon transmissions collides with particles of the scattering medium and reaches the point S. It can be described by the law of total probability as follows:

$$P(s) = \sum_{m=0}^{\infty} P_m(s). \tag{26}$$

The probability of photons arriving at point S of phase space after m times collisions is $P_m(s)$. It corresponds to $I_m(s)$ in equation (25).

The history of photon propagations and collisions can be described as $\{s_l\}(l = 0, 1, 2, \ldots, \mathrm{m})$, and arbitrary events $P_m(s) = P(s_0 s_1 \ldots s_{m-1} s_m) > 0$, because

$$P(s_0) \geq P(s_0 s_1) \geq \cdots \geq P(s_0 s_1 \ldots s_{m-1} s_m) > 0, \tag{27}$$

$$\begin{aligned} P(s_0 s_1 \cdots s_{m-1} s_m) &= P(s_0) P(s_1|s_0) P(s_2|s_0 s_1) \cdots P(s|s_0 s_1 \cdots s_{m-1}) \\ &= P(s_0) P(s_1|s_2) P(s_2|s_1) \cdots P(s_m|s_{m-1}). \end{aligned} \tag{28}$$

The latter term in equation (28) indicates that the random transmission of a photon in the medium are Markov processes. Comparing equations (25) with (28), the integral operator $\int K(s_{l-1} \longrightarrow s_l) \mathrm{d}s_{l-1}$ corresponds to the conditional probability $P(s_l|s_{l-1})$.

Using Monte Carlo simulation, the initial position of the incident photon is in the plane of $Z = 0$, as shown in Figure 1. For Lambert source, the probability sampling in the initial direction is $\mu_0 = \cos\theta_0 = \sqrt{\xi_1}$. ξ_i $(i = 1,2,3,4)$ is a random number uniformly distributed in the interval [0, 1].

The free path length L is the distance of a photon propagation until an interaction event, scattering, or absorption occurs, $\xi_2 = \exp(-Q_e L)$ means existence probability of photons after colliding with particles, Q_e is the extinction coefficient. The free path length L is as follow:

$$L = -\ln \frac{\xi_2}{Q_e}. \tag{29}$$

When scattering occurs, a new propagation direction must be specified, the H-G function is an appropriate phase function for fog particle scattering, the probability density function corresponding to normalized phase function is as follows [23]:

$$P(\nu) = \frac{(1 - g^2)(1 + g^2 - 2g\cos\nu)^{-3/2}}{4\pi}. \tag{30}$$

The scattering angle in the particle local coordinate system is ν and g is the asymmetry factor; the photon scattering direction is as follows:

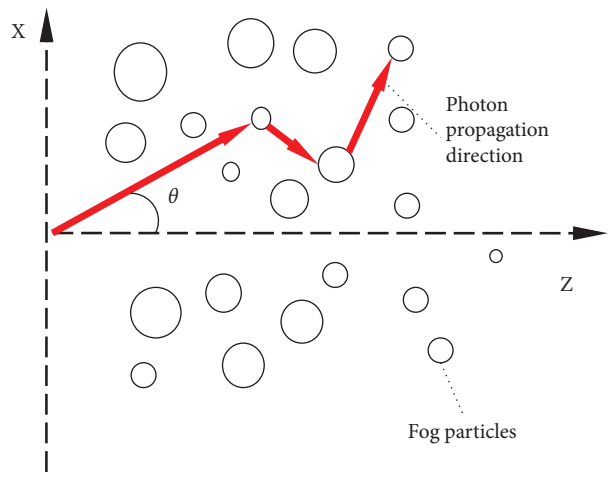

Figure 1: Photon propagation in the fog.

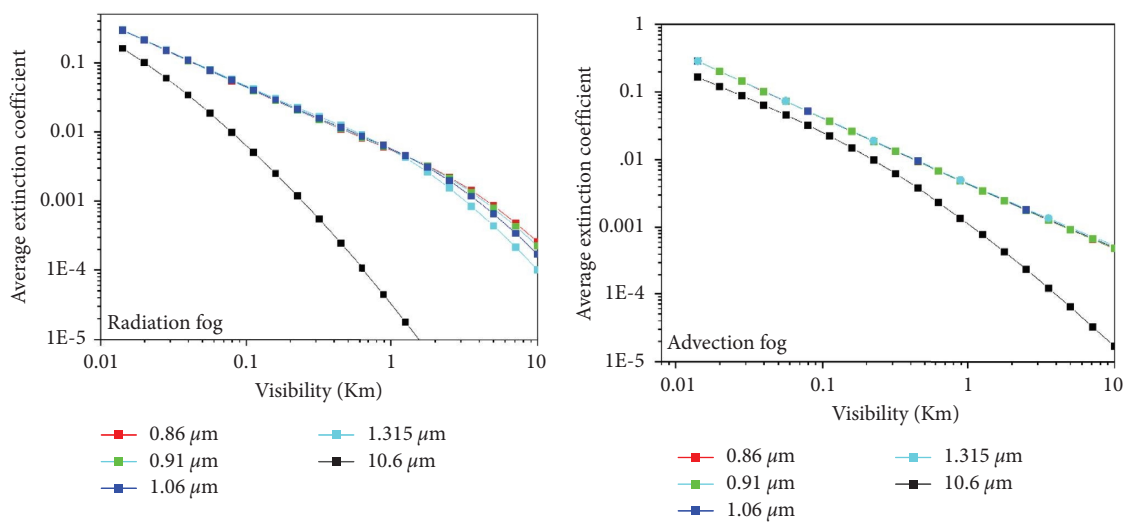

Figure 2: Average extinction coefficient versus visibility.

$$\cos\nu = \frac{\left[\left(1+g^2\right)-\left(1-g^2\right)^2/\left(1-g+2g\xi_3\right)^2\right]}{2g}, g \neq 0,$$

$$\cos\nu = 2\xi_3 - 1, g = 0. \tag{31}$$

By using the propagation distance L and scattering angle ν, the scattering direction and position of photons can be determined.

5. Calculation Results

Based on previous theories, the following calculations are proposed and advection fog and radiation fog are considered. The fog spectrum distribution is gamma distribution, as shown in equations (1)–(8). The value of visibility is between 0.01 km and 10 km. The laser wavelengths are 0.86 μm, 0.91 μm, 1.06 μm, 1.3015, and 10.6 μm, respectively. Firstly, we calculate the extinction coefficient, albedo, asymmetry factor of fog droplets versus visibility, then we use these parameters in the calculation of Monte Carlo method, the forward scattering and backscattering of laser light are calculated.

Figure 2 shows the average extinction coefficient of advection fog and radiation fog versus visibility at the light wavelength of 0.86 μm, 0.91 μm, 1.06 μm, 1.315 μm, and 10.6 μm. As shown in Figure 2, the average extinction coefficient decreases as the visibility increases, and the average extinction coefficient of advection fog is bigger than that of radiation fog under the same visibility. The average extinction coefficient fog is basically the same under the wavelength of 0.86 μm, 0.91 μm, 1.06 μm, and 1.315 μm. For wavelength of 10.6 μm, the average extinction coefficient is smaller than that of other wavelengths, and decreases quickly as visibility increases.

According to equations (16) and (19),

$$\langle \sigma_e \rangle = \frac{\pi \int_0^\infty r^2 Q_e(r) n(r) \mathrm{d}r}{\int_0^\infty n(r) \mathrm{d}r}, \tag{32}$$

$\langle \sigma_e \rangle$ mainly depends on Q_e and r. The droplet particle radius is much bigger than the wavelength of the incident light wave, so the change of Q_e is small, Q_e is close to 2. Therefore, the change trend of $\langle \sigma_e \rangle$ is mainly determined by r^2 in equation (16). From equations (9)–(11), it is shown that with the increase of V, r_0 decreases, $\bar{r}$ decreases, correspondingly r^2 decreases, so $\langle \sigma_e \rangle$ decreases. According to equation (15), Q_e contains parameter $2/a_\lambda{}^2$, $a_\lambda = 2\pi r/\lambda$, λ is wavelength, the wavelength of 10.6 μm is about 10 times bigger than other wavelengths (0.86 μm, 0.91 μm, 1.06 μm, and 1.315 μm), and its Q_e is calculated to be less than 2, which is smaller than that of other wavelengths, and with the same visibility, $\langle \sigma_e \rangle$ of 10.6 μm is smaller than that of other wavelengths.

Figure 3 shows the average albedo of advection fog and radiation fog versus visibility. It can be seen that the average albedo of wavelengths of 0.86 μm, 0.91 μm, 1.06 μm, and 1.315 μm in the two kinds of fog is close to 1. The average albedo of wavelength of 10.6 μm decreases as the visibility increases, it is obviously different from other wavelengths. Study on the refractive index of droplet of fog is as follows:

$$n = n' + in'', \tag{33}$$

where n' is the real part of the refractive index that represent the scattering capacity of the particle (Q_s) and n'' is the complex part that represents the absorption by the particle (Q_a). The extinction of the particle includes scattering and absorption ($Q_e = Q_s + Q_a$), as shown in Table 1, the refractive index is related to the wavelength of the incident wave.

For the wavelength of incident wave (0.86 μm, 0.91 μm, 1.06 μm, and 1.315 μm), the complex part of its refractive index is small, Q_a is small. According to equations (16)–(18), $\langle \sigma_a \rangle$ can be ignored, $\langle \sigma_e \rangle$ is close to $\langle \sigma_s \rangle$, and by equation (20), $\langle w_0 \rangle$ is approximately equal to 1. For the incident wave with wavelength of 10.6 μm. The complex part of refractive index is relatively big, $\langle \sigma_e \rangle$ is relatively big. The particle average size decreases with the increase of visibility, and particle size parameter $\alpha_\lambda = 2\pi r/\lambda$ is close to 1 and $\langle \sigma_s \rangle$ decreases rapidly, but $\langle \sigma_a \rangle$ changes slowly, so $\langle w_0 \rangle$ decrease as visibility increase.

Figure 4 shows the average asymmetry factor $\langle g \rangle$ of advection fog and radiation fog versus visibility. According to equation (21), average asymmetry factor $\langle g \rangle$ describes the relative proportion of forward and backward scattering energy of particles. When the incident wavelengths are 0.86 μm,0.91 μm, 1.06 μm, and 1.315 μm, the droplet particle radius is much bigger than the wavelength of the incident light wave. According to equation (21), the forward scattering is bigger, $\langle g \rangle$ is between 0.8 and 1. When the wavelength of incident light is 10.6 μm, and its real part of refractive index is smaller, $\langle g \rangle$ of this wavelength is slightly bigger than that of other wavelengths for lower visibility, with increasing of visibility. According to equation (10), $\bar{r}$ decreases, the particle size parameter $\alpha_\lambda = 2\pi r/\lambda$ is close to 1, forward scattering decrease, backward scattering increase, and $\langle g \rangle$ decreases rapidly.

Table 1: The refractive index of fog droplet related to the wavelength of the incident light.

Wavelength (μm)	Real part	Complex part
0.86	1.329	2.93×10^{-7}
0.91	1.323	5.70×10^{-7}
1.06	1.326	2.89×10^{-6}
1.315	1.316	1.639×10^{-5}
10.6	1.178	0.071

Asymmetry factor and albedo are important parameters for Monte Carlo calculation. The scattering intensity versus scattering angle is calculated according to these parameters. Combined with the numerical results of Mie theory, the foundation for calculating the attenuation and scattering of laser in fog is laid.

Figure 5 shows the change of forward scattering intensity and back scattering intensity with scattering angle, the laser wavelength is 1.06 μm, visibility is 0.1 km, the particle asymmetry factor $g = 0.75$, and w_0 is albedo. As shown in Figure 5(a), the forward scattering intensity increases when albedo increases, when the scattering angle is greater than 20°, the scattering intensity is relatively small, indicating that the forward scattering beam is relatively concentrated. As can be seen from Figure 5(b), the backward scattering intensity increases when single albedo increases, however, compared with the forward scattering intensity, the backward scatter intensity is much smaller. The backscattering intensity decreases when the scattering angle is larger than 60°, which indicates that the backscattering beams are more dispersed.

In Figure 6, the relationship between scattering intensity and scattering angle is calculated, particle albedo $w_0 = 0.9$. Figure 6(a) show that, the forward scattering increases when the asymmetry factor increases. The scattering intensity decreases when the scattering angle increases. It is shown in Figure 6(b), the backscattering intensity decreases when the asymmetry factor increases. At the same time, when the scattering angle is less than 50°, the scattering intensity changes little, and decreases with the increase of the scattering angle when the scattering angle is bigger than 50°. And the backward scatter intensity is much smaller than the forward scattering intensity.

Figure 7 shows the backscattering intensity versus scattering angle at several typical wavelengths when the visibility is 0.6 km. It can be seen from the Figure 7(a), for radiation fog, when the scattering angle is less than 40°, the scattering intensity oscillates rapidly, and there is little difference in the scattering intensity curves for wavelengths of 0.86 μm, 0.91 μm, and 1.06 μm. Figure 7(b) show that, for advection fog, the scattering intensity curves of 0.86 μm, 0.91 μm, and 1.06 μm of radiation fog are almost same. Comparing the two figures, it can be seen that the backscattering intensity of radiation fog is bigger than that of advection fog, and the backward scattering intensity of 10.6 μm is much smaller than that of other wavelengths, that means the forward transmittance of 10.6 μm is much bigger than that of other wavelengths.

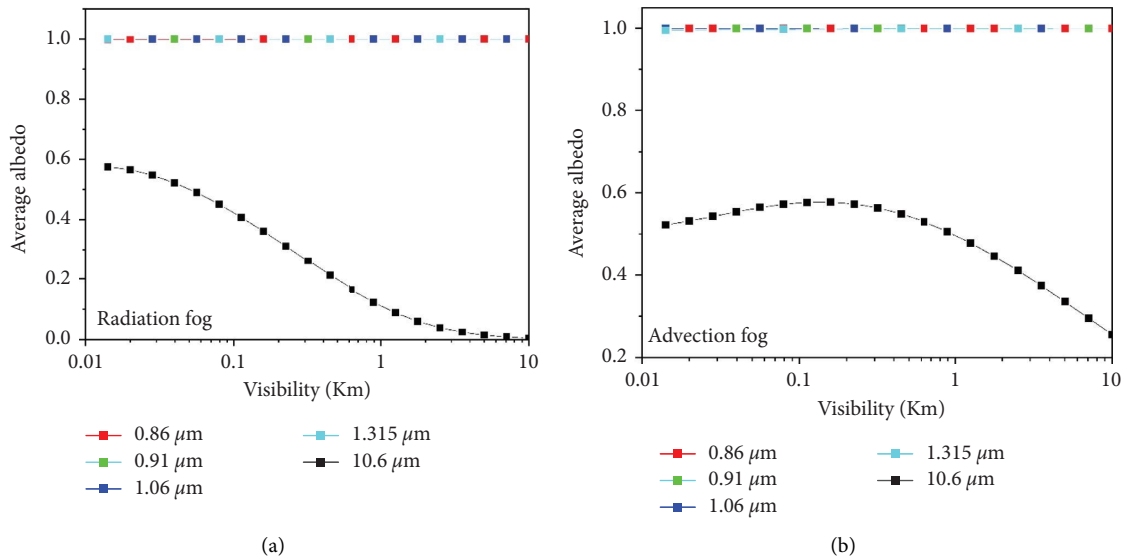

Figure 3: Average albedo versus visibility.

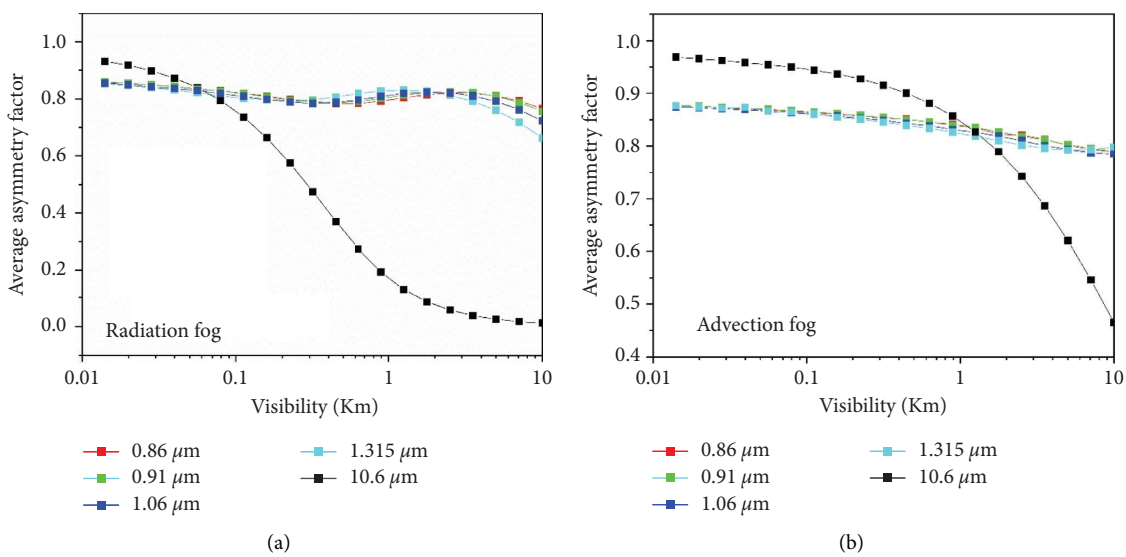

Figure 4: Average asymmetry factor versus visibility.

6. Summary

Based on the size distribution of fog, the scattering coefficient is calculated by Mie theory. The average extinction coefficient, albedo, and asymmetry factor of fogs versus visibility for the laser at wavelength of 0.86 μm, 0.91 μm, 1.06 μm, 1.315 μm, and 10.6 μm are discussed. The scattering coefficients are similar for the laser at the wavelength of 0.86 m, 0.91 μm, and 1.315 μm, but the coefficients of the laser at the wavelength of 10.6 μm are smaller. By the Monte Carlo method, correlations between of asymmetry factor, albedo, and scattering intensity are calculated. The forward and backward scattering intensity increases when the albedo increases. When the asymmetry factor increases, the forward scattering intensity increases, but the backscattering intensity decreases. The backward scattering intensity of radiation fog is bigger than advection fog for same visibility, and the backward scattering intensity of 10.6 μm is much smaller than that of other wavelengths. Compared with other studies, our model considers more parameters for the Monte Carl method and can precisely study beam propagation in fogs. This study can be applied to laser

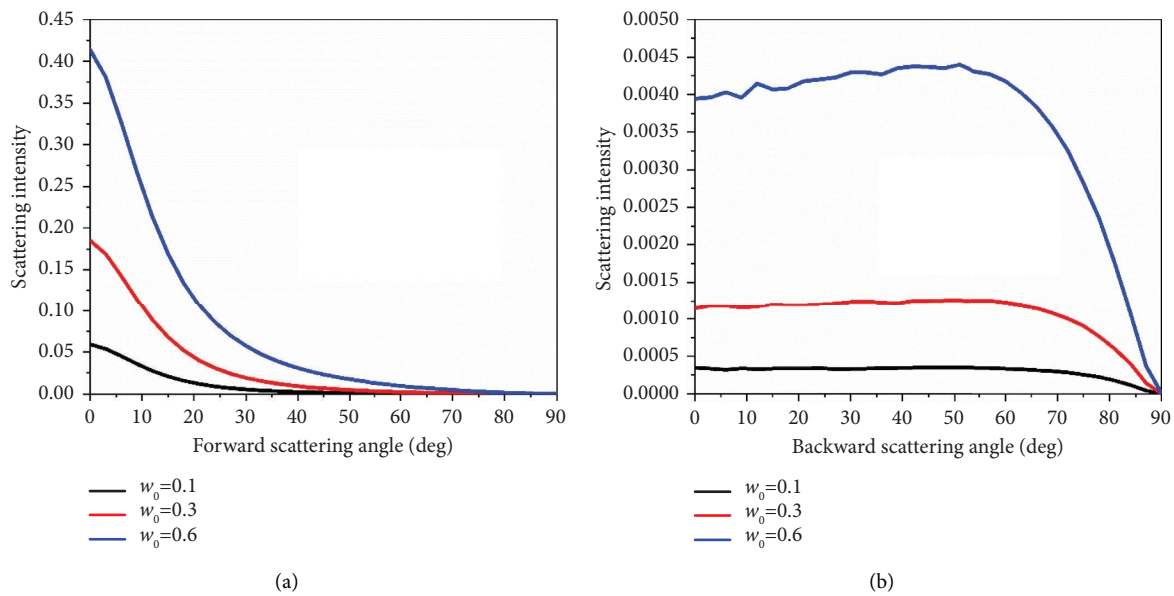

Figure 5: The scattering intensity versus scattering angle for different albedo.

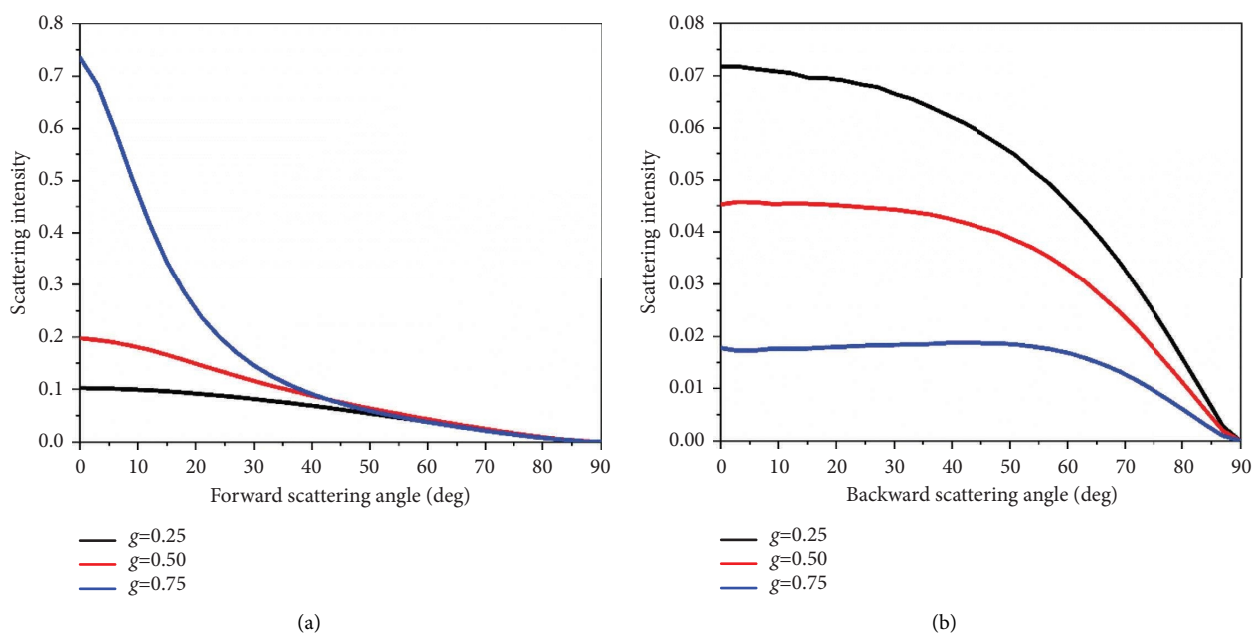

Figure 6: The scattering intensity versus scattering angle for different asymmetry factors.

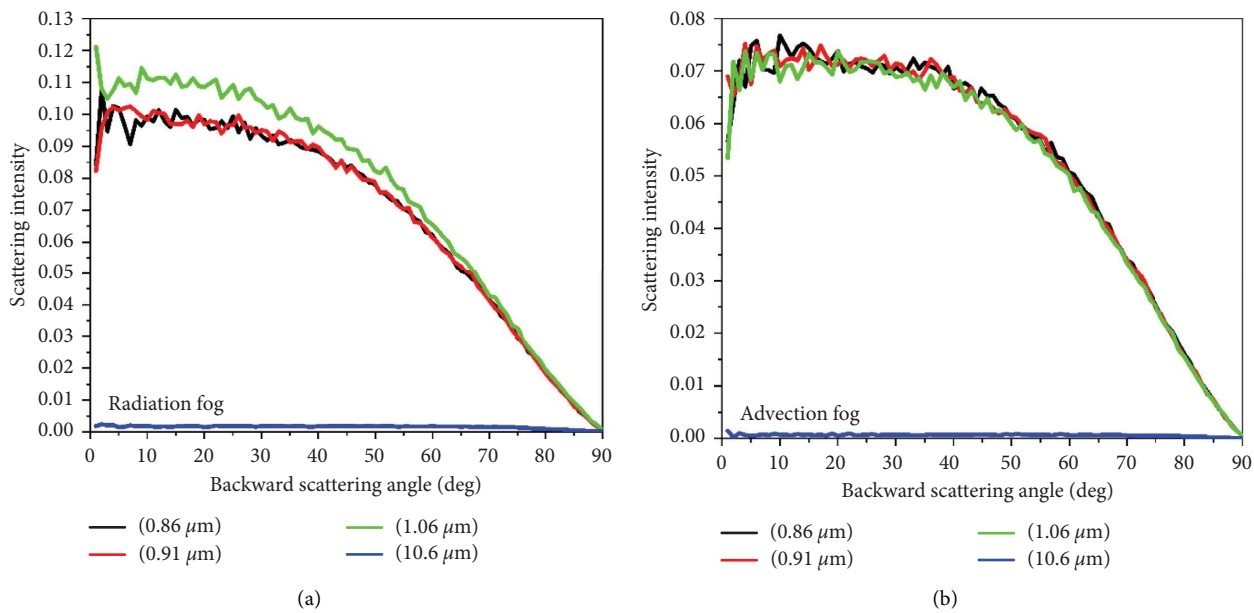

Figure 7: The backscattering intensity versus scattering angle for different wavelengths.

communication, laser remote sensing detection, and lidar detection in fog.

Data Availability

The data used to support the findings of this study are available from the corresponding author upon request.

Conflicts of Interest

The authors declare that they have no conflicts of interest.

Acknowledgments

The authors would like to thank the National Natural Science Foundation of China (61975158) and State Key Laboratory Fund (The State Key Laboratory of Transient Optics and Photonics, Xi'an Institute of Optics and Precision Mechanics).

References

[1] R. Nebuloni, "Empirical relationships between extinction coefficient and visibility in fog," *Applied Optics*, vol. 44, no. 18, pp. 3795–3804, 2005.

[2] M. Grabner and V. Kvicera, "Case study of fog attenuation on 830 nm and 1550 nm free-space optical links," in *Proceedings of the European Conference on Antennas & Propagation*, pp. 1–4, Barcelona, Spain, May 2010.

[3] R. Nebuloni and C. Capsoni, "Sensitivity of laser attenuation through fog to the wavelength and to the drop size distribution," in *Proceedings of the European Conference on Networks and Optical Communications*, pp. 86–90, Milan, Italy, December 2014.

[4] M. Ijaz, Z. Ghassemlooy, J. Pesek, O. Fiser, H. Le Minh, and E. Bentley, "Modeling of fog and smoke attenuation in free space optical communications link under controlled laboratory conditions," *Journal of Lightwave Technology*, vol. 31, no. 11, pp. 1720–1726, 2013.

[5] M. Grabner and V. Kvicera, "Multiple scattering in rain and fog on free-space optical links," *Journal of Lightwave Technology*, vol. 32, no. 3, pp. 513–520, 2014.

[6] S. Mori and F. S. Marzano, "Microphysical characterization of free space optical link due to hydrometeor and fog effects," *Applied Optics*, vol. 54, no. 22, pp. 6787–6803, 2015.

[7] X. Wu, H. Wang, and B. Song, "Measurement of fog and haze extinction characteristics and availability evaluation of free space optical link under the sea surface environment," *Applied Optics*, vol. 54, no. 5, pp. 1015–1026, 2015.

[8] M. Al Naboulsi and H. Sizun, "Measured and predicted light attenuation in dense coastal upslope fog at 650, 850, and 950 nm for free-space optics applications," *Optical Engineering*, vol. 47, no. 3, pp. 036001–036014, 2008.

[9] J. H. Shapiro, "Quasi-monochromatic bound on ultrashort light-pulse transmission through fog," *Optics Letters*, vol. 36, no. 17, pp. 3356–3358, 2011.

[10] K. Su, L. Moeller, R. B. Barat, and J. F. Federici, "Experimental comparison of performance degradation from terahertz and infrared wireless links in fog," *Journal of the Optical Society of America A*, vol. 29, no. 2, pp. 179–184, 2012.

[11] S. Shah, S. Mughal, and S. Memon, "Theoretical and empirical based extinction coefficients for fog attenuation in terms of visibility at 850 nm," in *Proceedings of the International Conference on Emerging Technologies*, pp. 1–4, Peshawar, Pakistan, December 2015.

[12] Y. Wang, J. Zhang, Q. Fu et al., "Variations in the water vapor distribution and the associated effects on fog and haze events over Xi'an based on Raman lidar data and back trajectories," *Applied Optics*, vol. 56, no. 28, pp. 7927–7938, 2017.

[13] H. Di, Z. Wang, and D. Hua, "Precise size distribution measurement of aerosol particles and fog droplets in the open atmosphere," *Optics Express*, vol. 27, no. 12, pp. A890–A908, 2019.

[14] X. Zeng, J. Chu, W. Cao, W. Kang, and R. Zhang, "Visible-IR transmission enhancement through fog using circularly

polarized light," *Applied Optics*, vol. 57, no. 23, pp. 6817–6822, 2018.

[15] C. Zhang, J. Zhang, X. Wu, and M. Huang, "Numerical analysis of light reflection and transmission in poly-disperse sea fog," *Optics Express*, vol. 28, no. 17, pp. 25410–25430, 2020.

[16] H. Vasseur and C. J. Gibbins, "Inference of fog characteristics from attenuation measurements at millimeter and optical wavelengths," *Radio Science*, vol. 31, no. 5, pp. 1089–1097, 1996.

[17] M. Al Naboulsi, H. Sizun, and F. Fornel, "Fog attenuation prediction for optical and infrared waves," *Optical Engineering*, vol. 43, no. 2, pp. 319–329, 2004.

[18] E. M. Patterson, D. A. Gillette, and G. W. Grams, "The relation between visibility and the size-number distribution of airborne soil particles," *Journal of Applied Meteorology*, vol. 15, no. 5, pp. 470–478, 1976.

[19] L. J. Ippolito, R. D. Kaul, and R. G. Wallace, *Propagation Effects Handbook for Satellite Systems Design*, NASA Reference Publication, Washington, DC, USA, 1983.

[20] M. Wendisch and P. Yang, *Theory of Atmospheric Radiative Transfer*, Wiley-Vch press, New, York, NY, USA, 2012.

[21] A. Kokhanovsky and E. Zege, "Optical properties of aerosol particles: a review of approximate analytical solutions," *Journal of Aerosol Science*, vol. 28, no. 1, pp. 1–21, 1997.

[22] L. Bai, Z. S. Wu, H. Y. Li, and T. Li, "Scalar radiative transfer in discrete media with random oriented prolate spheroids particles," *Progress In Electromagnetics Research B*, vol. 33, pp. 21–44, 2011.

[23] D. Toublanc, "Henyey-Greenstein and mie phase functions in Monte Carlo radiative transfer computations," *Applied Optics*, vol. 35, no. 18, pp. 3270–3274, 1996.